

4D Radar Ground Truth Augmentation with LiDAR-to-4D Radar Data Synthesis

Woo-Jin Jung, Dong-Hee Paek, and Seung-Hyun Kong*

*^aCCS Graduate School of Mobility, Korea Advanced Institute of Science and
Technology, 193, Munji-ro, Yuseong-gu, Daejeon, 34051, Daejeon, Republic of Korea*

Abstract

Ground truth augmentation (GT-Aug) is a common method for LiDAR-based object detection, as it enhances object density by leveraging ground truth bounding boxes (GT bboxes). However, directly applying GT-Aug to 4D Radar tensor data overlooks important measurements outside the GT bboxes—such as sidelobes—leading to synthetic distributions that deviate from real-world 4D Radar data. To address this limitation, we propose 4D Radar Ground Truth Augmentation (4DR GT-Aug). Our approach first augments LiDAR data and then converts it to 4D Radar data via a LiDAR-to-4D Radar data synthesis (L2RDaS) module, which explicitly accounts for measurements both inside and outside GT bboxes. In doing so, it produces 4D Radar data distributions that more closely resemble real-world measurements, thereby improving object detection accuracy. Experiments on the K-Radar dataset show that the proposed method achieves improved performance compared to conventional GT-Aug in object detection for 4D Radar. The implementation code is available at <https://github.com/kaist-avelab/K-Radar>.

Keywords: 4D Radar, Ground Truth Augmentation, 4D Radar Synthesis, Generative Adversarial Networks

1. Introduction

Object detection is a core component of autonomous driving systems, providing essential information about the location and class of surrounding objects for effective path planning and control. Robust detection—defined as maintaining consistent and accurate performance across various environmental and weather conditions—is vital for reliable operation. Although

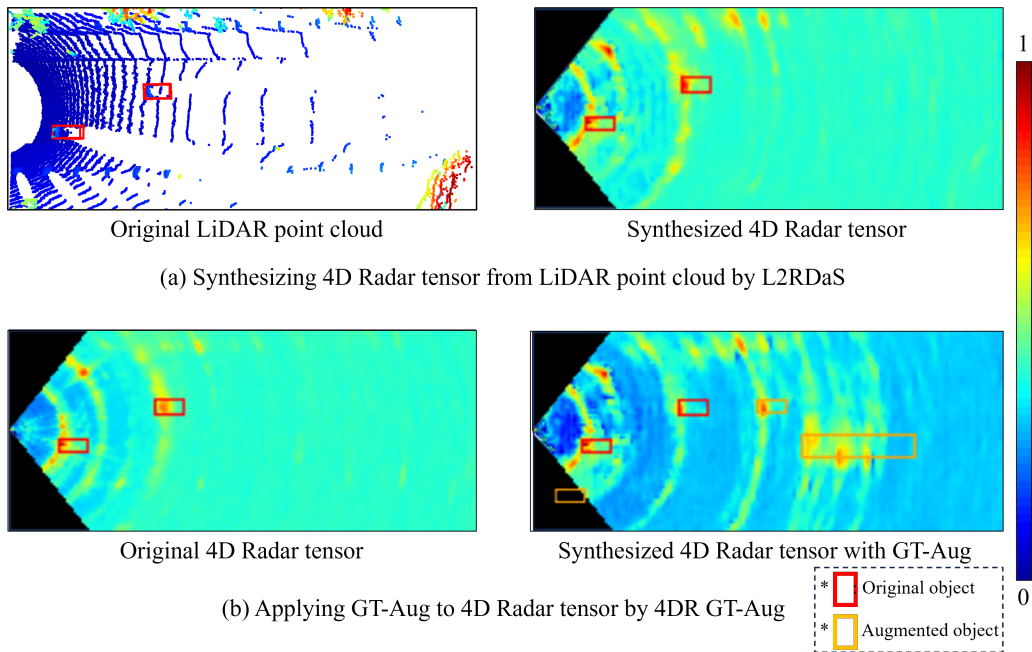


Figure 1: The key contributions of our work. The LiDAR data is represented in a Bird’s Eye View (BEV) format, where colors indicate normalized height values. The 4D Radar tensor is visualized as a heatmap by applying mean pooling along both the Doppler and height axes, with colors representing normalized power values. All data in the figure corresponds to the same frame. In (a), the first contribution is demonstrated, where the proposed L2RDaS module enables the synthesis of 4D Radar tensor data from LiDAR input. In (b), the second contribution is shown, where 4DR GT-Aug is applied to the 4D Radar tensor, allowing for enhanced data augmentation.

cameras and LiDAR sensors are widely used in autonomous driving, their performance degrades in adverse weather because they rely on visible and near-infrared light. In contrast, conventional Radar systems typically rely on millimeter-wave signals to measure range, Doppler, and azimuth angles, enabling them to penetrate rain and snow particle and thereby provide more robust detection performance. Recent hardware developments have led to 4D Radar, which expands on conventional Radar by incorporating elevation antennas. This facilitates measurement of range, azimuth, Doppler, and elevation, allowing extraction of full 3D structural information [1].

A key factor among various data-related strategies for improving object detection performance is object density, defined as the average number of labeled objects per frame. A higher object density increases the diversity

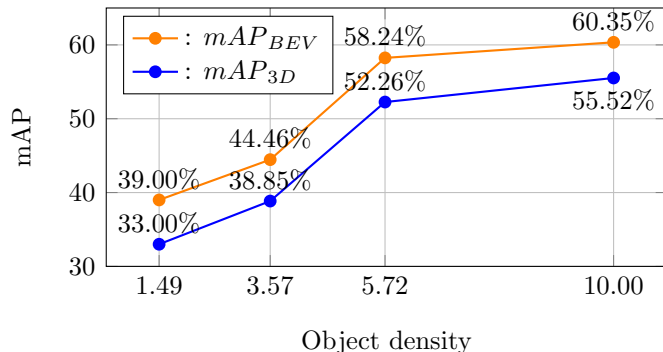


Figure 2: Effect of object density on detection performance. This graph illustrates the relationship between object density and detection accuracy using LiDAR data from the K-Radar dataset [2] and the SECOND object detection model [3]. The x-axis represents object density, defined as the average number of labeled objects per frame, while the y-axis shows mean Average Precision (mAP), measuring detection performance. The data points at densities 1.49, 3.57, and 5.72 correspond to the original LiDAR dataset, whereas the highest density (10.00) was achieved using LiDAR Ground Truth Augmentation (GT-Aug). The results indicate that increasing object density leads to improved detection accuracy in both BEV and 3D object detection.

of labeled samples, enabling the model to learn a broader range of object poses and characteristics, which enhances feature representation [4]. Additionally, as shown in Fig. 1 (b), increasing object density results in more objects appearing within a single frame, naturally leading to denser scenes with occlusions and multi-object interactions. These factors provide complex contextual information, contributing to better generalization and robustness [5]. To verify the impact of object density, we conducted experiments using LiDAR data from the K-Radar dataset [2], which contains autonomous driving data collected using LiDAR, 4D Radar, and cameras, as shown in Fig. 2. We trained the SECOND model [3], a widely used LiDAR detection network, on datasets with the same number of frames but varying object densities, including cases where we artificially increased the density through sampling. The results confirm that a higher object density indeed improves detection performance. However, collecting large-scale, high-density datasets is both time-consuming and expensive. In LiDAR-based detection, ground truth augmentation (GT-Aug) is commonly used to alleviate this problem by increasing object density through copying and pasting ground truth bounding boxes (GT bboxes) from external frames into the current scene [3, 6]. Throughout this paper, we refer to this as conventional GT-Aug to distin-

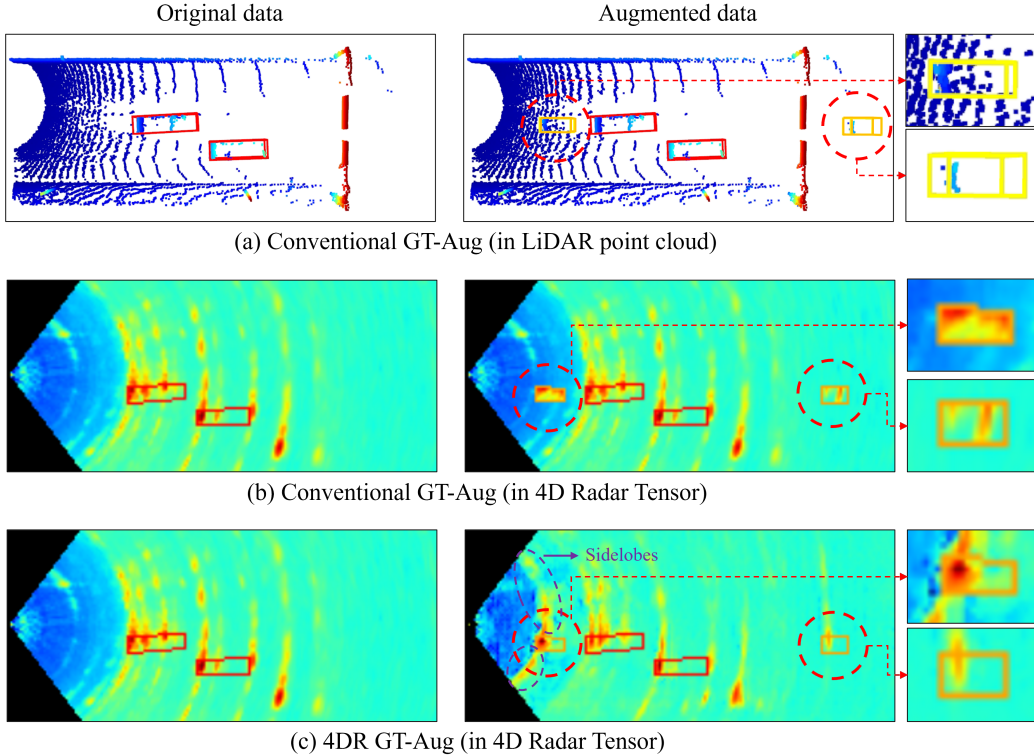


Figure 3: Comparison of conventional GT-Aug and 4DR GT-Aug. (a) illustrates Conventional GT-Aug applied to LiDAR point cloud data. (b) shows the direct application of Conventional GT-Aug to 4D Radar tensor data, which results in a fragmented appearance and lacks sidelobes. (c) demonstrates the proposed 4DR GT-Aug, where power distribution is not limited to the inside of object bboxes but extends beyond, reflecting radar-specific characteristics such as sidelobes. This ensures that the augmented data does not solely emphasize high-power regions within object bboxes but also captures realistic surrounding patterns, making it more representative of actual radar measurements.

guish it from our proposed method.

Nevertheless, applying conventional GT-Aug to 4D Radar data is unsuitable due to inherent challenges. Conventional GT-Aug relies solely on points within GT bboxes (Fig. 3 (a)), excluding measurements outside them, which is problematic for 4D Radar. One key challenge is 4D Radar’s lower angular resolution, which often causes measurements to extend beyond GT bboxes. To maintain compactness and lightweight design, automotive 4D Radars have a limited number of antennas, resulting in an angular resolution of 1–2° horizontally and 2–3° vertically [7], compared to 0.7° horizontally and

0.18° vertically in LiDAR sensors [8]. This coarser resolution spreads object measurements beyond actual boundaries[9]. Another challenge arises when applying conventional GT-Aug to 4D Radar tensor data, as it fails to account for sidelobes, leading to a distribution that deviates from real-world 4D Radar measurements, as shown in Fig. 3 (b). 4D Radar tensor data are expressed in the frequency-domain power distribution across range, azimuth, elevation, and Doppler, serving as the raw representation before point cloud generation. Sidelobes—secondary energy patterns surrounding actual objects—are inherently present in tensor data and become more pronounced as the radar cross-section (RCS) increases. However, if sidelobes are not properly incorporated during augmentation, the generated training data may fail to reflect real-world 4D Radar distributions, reducing reliability and consistency in practical applications. The characteristics and causes of sidelobes will be discussed in Section 2.

To enhance the applicability of GT-Aug in 4D Radar tensor data, we propose 4D Radar GT-Aug (4DR GT-Aug), which explicitly addresses measurement extensions beyond GT bboxes and the lack of sidelobe representation, as shown in Fig. 3 (c). This method first increases object density in LiDAR data using conventional GT-Aug and then converts it into 4D Radar data via the LiDAR-to-4D Radar data synthesis (L2RDaS) module, ensuring effective augmentation for 4D Radar tensor data. We apply conventional GT-Aug on LiDAR data because direct object copy-pasting is impractical in radar data due to angular resolution limitations and sidelobe effects. In contrast, LiDAR enables direct copying and pasting of objects within the point cloud, and allows us to leverage existing methods. To transform LiDAR data into radar data, we employ a conditional generative adversarial networks (cGANs) based generative model that learns radar-specific features from LiDAR. Since direct object copy-pasting is impractical in radar data, we adopt a domain translation approach, as demonstrated in Pix2Pix[10] and Pix2PixHD[11], which have been widely used for mapping one domain to another. Among such methods, L2R[12] is a representative approach that applies GAN-based transformation specifically for converting LiDAR data into radar data. Given this similarity, our method builds upon L2R’s generative modeling strategy, adapting it to synthesize 4D Radar data from augmented LiDAR data, ensuring that GT-Aug can be effectively applied in the radar domain.

To evaluate the effectiveness of 4DR GT-Aug, we applied it to the K-Radar dataset [2], which is the only dataset providing 4D Radar tensor data,

and tested it with RTNH [2], the only baseline model that performs 4D Radar-only object detection directly on 4D Radar tensor data. While various studies [13, 14] have utilized the K-Radar dataset, RTNH remains the primary baseline model for evaluating 4D Radar-based object detection, making it the most suitable benchmark for assessing the proposed augmentation method. The results showed that 4DR GT-Aug improved RTNH object detection performance. Compared to no augmentation, 4DR GT-Aug increased BEV performance by 4.8 percentage points and 3D performance by 1.54 percentage points. Additionally, compared to conventional GT-Aug on 4D Radar, BEV performance increased by 1.54 percentage points, and 3D performance improved by 0.61 percentage points. These results confirm the effectiveness of 4DR GT-Aug in performing GT-Aug for 4D Radar tensor data. The proposed method is expected to contribute to the advancement of 4D Radar-based perception technologies in autonomous driving.

The main contributions of this study are as follows:

- Proposing L2RDaS, the first method for synthesizing 4D Radar tensor data with 3D spatial information from LiDAR point clouds.
- Introducing 4DR GT-Aug, the first GT-Aug method specifically developed for 4D Radar tensor data, incorporating both inside and outside GT bboxes.
- Demonstrating that the proposed 4DR GT-Aug improves RTNH performance, achieving a 4.8 percentage point increase in BEV and 1.54 percentage point increase in 3D detection over no augmentation, while surpassing conventional GT-Aug by 1.54 percentage points in BEV and 0.61 percentage points in 3D.

This paper is organized as follows. Section 2 examines the characteristics and causes of sidelobes. Section 3 reviews previous studies related to L2RDaS. Section 4 provides a detailed explanation of the proposed 4DR GT-Aug pipeline, including its structure and implementation. Section 5 presents quantitative and qualitative experimental results, along with an ablation study. Finally, Section 6 concludes the study and discusses future research directions.

2. Sidelobes background

This section explains the causes and characteristics of sidelobes through Radar signal processing.

Sidelobes refer to unnecessary spectral components appearing in the peripheral regions of the frequency spectrum, excluding the main lobe, which represents the central region containing the majority of the signal's power, as shown in Fig. 1. They are formed by deterministic factors such as the power spectral density (PSD) and non-deterministic factors like noise [15]. The Radar signal's bandwidth, time-domain waveform, and window function selection influence the PSD, determining the size and shape of sidelobes. For instance, in the frequency-modulated continuous wave (FMCW) method commonly used in 4D Radar, linearly modulated chirp signals are transmitted, and the frequency difference between the transmitted and reflected signals is processed using range fast Fourier transform (FFT) to estimate object distance. Doppler FFT is then applied to measure relative velocity, and angle FFT identifies object directions [16]. During this process, sidelobes, inherent characteristics of Radar, appear in the frequency spectrum through FFT. FFT is widely used to transform time-domain signals into the frequency domain. However, because FFT assumes infinite repetition of finite signals, spectral leakage can occur. To mitigate this, window functions are applied to smooth and limit signals, influencing the size and shape of sidelobes. For example, using a rectangular window preserves the time-domain signal but generates high sidelobes, increasing spectral distortion in the frequency spectrum. The rectangular window can be expressed in the frequency domain as the Dirichlet Kernel (Equation 1).

$$W[k] = \frac{\sin(\pi k)}{\sin\left(\frac{\pi k}{N}\right)} e^{-j\pi \frac{N-1}{N}k}, \quad (1)$$

where N represents the number of samples. The main lobe concentrates energy around the center frequency, while sidelobes distribute energy in surrounding areas. When $N \gg 1$ and $|k| \ll N$, the Dirichlet Kernel approximates a scaled sinc function. Using alternative window functions, such as Hann [17] or Blackman [18] can reduce sidelobe size but broadens the main lobe, creating a trade-off. Therefore, selecting a window function suitable for the measurement environment and analysis objectives is crucial to effectively control sidelobes. When a window function is applied, multiplying the time-domain signal by the window function results in the convolution of the

signal spectrum and the window function spectrum in the frequency domain, ultimately yielding the desired signal spectrum [19].

3. Related Work

This section reviews prior research on radar data generation techniques, focusing on methods that synthesize radar data from different modalities. These approaches can be broadly categorized into radar tensor generation and radar point cloud generation. Additionally, we review image translation models, which serve as a foundational framework for developing the proposed method.

3.1. Radar Data Generation from Different Modalities

Several methods have been proposed to generate radar tensor data, primarily in the form of 2D radar maps (e.g., Range-Doppler or Range-Azimuth maps). Weston et al. [20] translate elevation maps into simulated radar observations using adversarial training and cyclic consistency loss to enhance realism. L2R GAN [12] converts LiDAR point clouds into BEV images and subsequently into radar spectra using an occupancy-grid-mask-guided global generator and a local region generator through adversarial training. Fidelis [21] employs a GAN-based approach to synthesize raw FMCW radar data, generating 16 simultaneous chirps, which are then used to construct Range-Azimuth (RA) maps for downstream processing. RadSimReal [22] introduces a physical radar simulation framework that generates synthetic radar images with annotations. RAIDS [23] presents an image-to-radar range-azimuth (RA) map estimation model that incorporates depth and semantic descriptions to enhance the accuracy of generated radar maps.

Additionally, LiDAR-to-Radar Translation [24] maps LiDAR point clouds to radar point clouds using a voxel feature extraction module. Alkanat [25] estimates radar point cloud probability distributions (PDFs) from camera images using CNN-based density estimation techniques, enabling the generation of high-density synthetic radar point clouds.

Existing radar tensor generation methods are primarily limited to 2D radar maps, lacking extensions to higher-dimensional representations. Additionally, most 4D Radar point clouds are provided using CFAR-based methods, which are not well-suited for deep learning [26]. As a result, generating structured 4D Radar tensor data presents a more promising approach for

radar-based learning. Furthermore, previous radar tensor generation techniques have primarily relied on cGANs-based methods, originally developed for image translation. Building upon these approaches, we extend beyond conventional 2D representations to synthesize structured 4D Radar tensor data tailored for deep learning applications.

3.2. Image translation

Image translation focuses on style translation while preserving key information. Notable methods include pix2pix [10] and pix2pixHD [11]. These methods utilize cGANs to translate input images into output images. Pix2pix employs a U-Net-based generator and a patch-based discriminator, enabling applications such as image synthesis and color translation. Pix2pixHD extends this framework to handle high-resolution images by incorporating boundary maps, multi-scale generators, and multi-scale discriminators, achieving improved quality.

These methods excel at 2D image-to-image translation while maintaining structural information. However, L2RDaS in this study aims to translate 3D LiDAR point cloud into 4D Radar tensor, rendering the direct use of traditional image translation models inadequate. To address this, this study extends the pix2pixHD framework by designing structural modifications to effectively process 3D data.

4. Method

This study proposes the 4DR GT-Aug method, which synthesizes 4D Radar tensor data reflecting measurements both inside and outside GT bboxes, leveraging this data in training to improve object detection performance. To achieve this, two key tasks were performed: (1) the design of the L2RDaS, which synthesizes LiDAR point cloud data into 4D Radar tensor data (Fig. 4 (a)); and (2) the construction of a 4DR GT-Aug pipeline integrating auxiliary modules such as OBIS, Paste box, and Switcher (Fig. 4 (b)). This section explains the roles and implementation of each component.

4.1. Design of the L2RDaS Module

The L2RDaS is the key module of 4DR GT-Aug pipeline, responsible for synthesizing 4D Radar tensor data from LiDAR point cloud. This module creates 4D Radar tensor data that reflects measurements both inside and

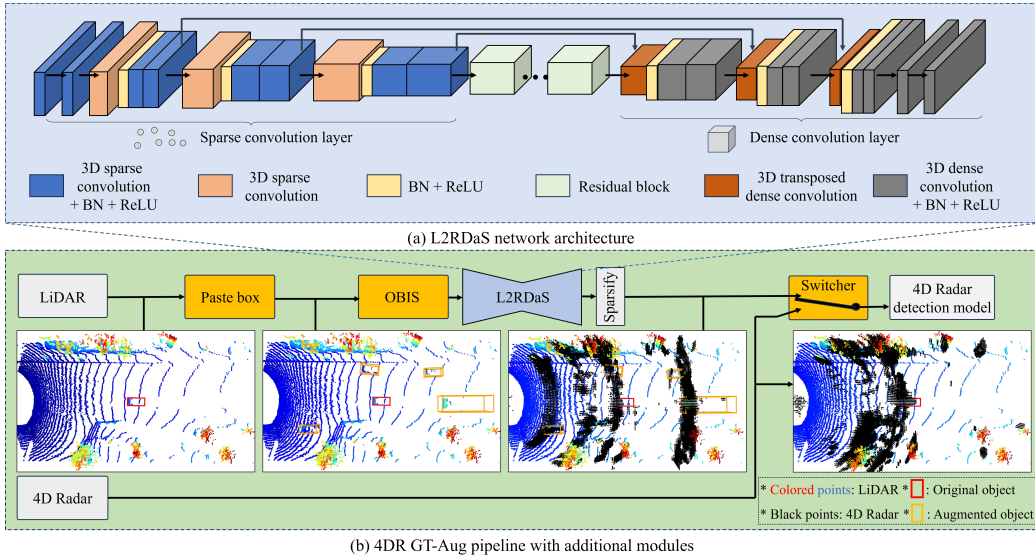


Figure 4: Overall 4D Radar GT-Aug pipeline. (a) illustrates the network structure of the L2RDaS, which translates LiDAR data into 4D Radar tensors using 3D sparse convolution in the encoder and 3D dense convolution in the decoder. Note that (a) depicts only the generator trained using cGAN, while the discriminator is omitted for clarity. (b) illustrates the 4DR GT-Aug pipeline, comprising L2RDaS, OBIS, and other auxiliary modules. OBIS provides additional object information to help L2RDaS synthesize 4D Radar tensors with distributions similar to actual Radar data. The constructed pipeline supports object augmentation effectively for 4D Radar.

outside GT bboxes, resulting in data distributions similar to actual measurement data. While the conventional GT-Aug, as shown in Fig. 3 (b), utilizes only points inside GT bboxes failing to include measurements outside them, the L2RDaS overcomes this limitation as shown in Fig. 3 (c).

4.1.1. Details of Encoder-Decoder

As mentioned in Section 3.2, the L2RDaS is built upon the generator structures of pix2pix [10] and pix2pixHD [11], restructured to synthesize 4D Radar tensor data from 3D LiDAR point cloud. While the referenced models process 2D data, L2RDaS has been modified to handle 3D data by adapting its encoder and decoder to a 3D data structure.

In this study, the synthesized 4D Radar data is structured as a three-dimensional tensor by applying mean pooling along the Doppler axis. This format was chosen to effectively capture the distribution of 4D Radar measurements while maintaining flexibility for point cloud generation, reducing

model complexity, and validating the feasibility of 4D Radar tensor synthesis. The original four-dimensional tensor, which includes the Doppler axis, would require handling temporal variations and additional processing for temporal information, further increasing model complexity.

To effectively extract the spatial characteristics of input data, the encoding method of Voxelnet [27], as referenced in Lee [24], was applied. The L2RDaS builds upon the U-net [28] structure used in traditional image translation but has been restructured to process 3D data.

As shown in Fig. 4 (a), the encoder uses 3D sparse convolution layers to account for the sparsity of LiDAR point cloud data. Sparse convolution layers [29] are used to reduce spatial dimensions, while submanifold sparse convolution layers [30] are used to enhance features without changing spatial dimensions. The decoder utilizes 3D dense convolution layers to synthesize dense 3D tensors, suitable for performing computations across all regions and producing complete tensors.

The synthesized tensor data is evaluated by a multi-scale discriminator [11], which determines its authenticity. To handle dense data, the discriminator also uses 3D dense convolution layers.

4.1.2. Objective functions

L2RDaS adopts a training framework using a Generator (G) and a Discriminator (D), inspired by traditional image translation methods. While image translation typically aims for a one-to-many mapping to generate diverse outputs, this study focuses on a one-to-one mapping, necessitating the design of appropriate loss functions. Following the method by Wang [12], the final loss function is defined as follows:

$$\mathcal{L}(G, D) = \mathcal{L}_{cGAN}(G, D) + \lambda_{L1}\mathcal{L}_{L1}(G) + \lambda_{perc}\mathcal{L}_{perc}(G) \quad (2)$$

where λ_{L1} and λ_{perc} are weights that control the importance of each loss component, ensuring balanced training.

First, a conditional adversarial loss is used, where the G synthesizes data, and the D learns to distinguish between real and synthesized data. This is the core loss of Conditional GANs, defined as:

$$\mathcal{L}_{cGAN}(G, D) = \mathbb{E}_{x,y}[\log D(x, y)] + \mathbb{E}_x[\log(1 - D(x, G(x)))] \quad (3)$$

Here, x represents input data, y is the GT, and $G(x)$ is the output of the G . The D learns to differentiate $G(x)$ from y , while the $G(x)$ is trained to deceive D by making $G(x)$ resemble y .

Second, L1 loss minimizes the absolute error between synthesized data $G(x)$ and GT y . This simple and stable loss function ensures that the synthesized data closely resembles real data:

$$\mathcal{L}_{L1}(G) = \mathbb{E}_{x,y} [|G(x) - y|_1] \quad (4)$$

Third, perceptual loss introduced in pix2pixHD is used to compare high-level feature distributions between synthesized and real data. By leveraging intermediate layer outputs from a pre-trained neural network, perceptual loss measures semantic differences, guiding the synthesized data to have similar high-level features to real data.

4.1.3. Training

To apply the L2RDaS module for LiDAR-to-Radar transformation, the model is trained to learn the distribution of 4D Radar data. Since K-Radar [2] is the only dataset providing 4D Radar tensor data, it is used to train L2RDaS to capture the radar distribution effectively. The training region of interest (ROI) is defined based on the measurement range of the K-Radar system: $[0, 76.8]$, $[-38.4, 38.4]$, $[-2, 10.8]$ for the x , y , and z -axes, respectively. This configuration follows the ROI setup of RTNH, the only baseline model that performs object detection exclusively on 4D Radar tensor data. Since L2RDaS is designed to augment 4D Radar tensor data, it adopts a similar ROI configuration to RTNH, ensuring consistency in radar data processing. Additionally, the LiDAR data range is adjusted to align with 4D Radar measurements.

During training, the original LiDAR point cloud is input into L2RDaS, which synthesizes corresponding 4D Radar tensor data. The discriminator then compares the synthesized data with real radar data to distinguish between them. Through this adversarial learning process, L2RDaS progressively refines its ability to generate realistic 4D Radar data distributions.

Once trained, L2RDaS is integrated into the 4DR GT-Aug pipeline to facilitate data augmentation, ultimately enhancing object detection performance on 4D Radar tensor data.

4.2. 4DR GT-Aug Pipeline with Additional Modules

To generate augmented data that includes measurements outside GT bboxes in 4D Radar data and effectively utilize it in training, the 4DR GT-Aug pipeline was constructed as shown in Fig. 4 (b). This pipeline integrates

the OBIS and other auxiliary modules (Paste box and Switcher). The OBIS provides additional object information to L2RDaS, aiding in synthesizing 4D Radar data distributions similar to real-world measurements. The auxiliary modules are incorporated into the pipeline to enhance object detection performance through 4DR GT-Aug. The following sections explain each component in the order of the pipeline.

4.2.1. *Paste box*

The Paste box module applies conventional GT-Aug [3] to LiDAR data to generate augmented LiDAR data with increased object density. This augmented data is then translated into 4D Radar tensor data through L2RDaS and utilized for object detection model training. The Paste box is highly flexible, allowing various LiDAR data augmentation methods [31, 32, 33] to be applied. In this study, the method proposed in [3] was employed. This technique randomly selects points within GT bboxes from other frames and adds them to the current frame, increasing object density and expanding its spatial distribution.

4.2.2. *OBIS*

The OBIS enhances the quality of 4D Radar data generated by the L2RDaS by providing object information for realistic data distribution. It addresses two key issues in synthesizing 4D Radar data: (1) the inability to clearly distinguish objects from the background as shown in Fig. 5 (d), and (2) synthesis errors when objects are closely spaced, as shown in Fig. 5 (b). To resolve these issues, OBIS enriches the LiDAR point cloud with additional object information.

For issue (1), two channels were added to the LiDAR point cloud to explicitly define whether a point lies within the bounding box of a Sedan or a Bus/Truck, which are the object classes used for detection in the K-Radar dataset. This allows L2RDaS to better interpret LiDAR measurements, separating objects from the background and generating synthetic data that closely resembles real-world measurements.

For issue (2), points were generated at regular intervals along bounding box boundaries. Inspired by the boundary map in pix2pixHD [11], this method delineates boundaries between closely positioned objects, avoiding misinterpretation. The added points, with intensities set to 0, were explicitly marked as bounding box representations via a new channel in the LiDAR point cloud.

As a result, the OBIS adds three channels to the LiDAR point cloud data: (1) whether a point is inside a Sedan GT bbox, (2) whether a point is inside a Bus/Truck GT bbox, and (3) whether a point represents a bounding box boundary. By integrating these channels, the OBIS helps L2RDaS distinguish objects from the background and accurately interpret closely spaced objects, enabling the synthesis of 4D Radar data that closely resembles real-world measurement distributions.

4.2.3. Switcher

The Switcher module optimizes the balance between original and synthesized data to enhance GT-Aug training performance. It is designed to prevent performance degradation caused by over-reliance on synthesized data and to address L2RDaS’s limitations in specific environments. According to research Shumailov et al. [34], training solely on synthesized data can increase data bias, reducing the model’s generalization performance. Switcher addresses this issue by incorporating original data into the training process. By balancing the use of original and synthesized data, it maintains the reliability and stability of the model, ensuring consistent performance even in complex scenarios.

L2RDaS struggles in environments such as tunnels and alleyways due to pronounced multi-path effects, as shown in Table 2. Multi-path occurs when electromagnetic waves reach the receiving antenna via multiple reflected paths, leading to distortions in radar measurements. To counteract this, Switcher selectively applies only original data in such environments while utilizing both original and synthesized data in other cases. This prevents erroneous object detection training resulting from L2RDaS’s performance degradation under specific conditions. This selective mechanism is feasible because K-Radar provides metadata descriptions indicating weather and road conditions for each data sample. Leveraging this metadata, Switcher differentiates between challenging environments (e.g., tunnels), ensuring synthesized data is used only when appropriate. In future work, we aim to enhance L2RDaS to achieve consistent synthesis performance across all road environments, thereby eliminating the need for selective switching and further improving training stability.

5. Experimental Results

This section demonstrates the effectiveness of 4DR GT-Aug. First, the dataset and implementation details used for training the L2RDaS and object detection models are described. Second, the evaluation metric for measuring performance in the experiments is explained. Third, the proposed method is compared with the conventional GT-Aug based on experimental results to evaluate its performance. Finally, ablation studies are conducted to analyze the impact of each module in the 4DR GT-Aug pipeline and to determine the optimal structure and configuration.

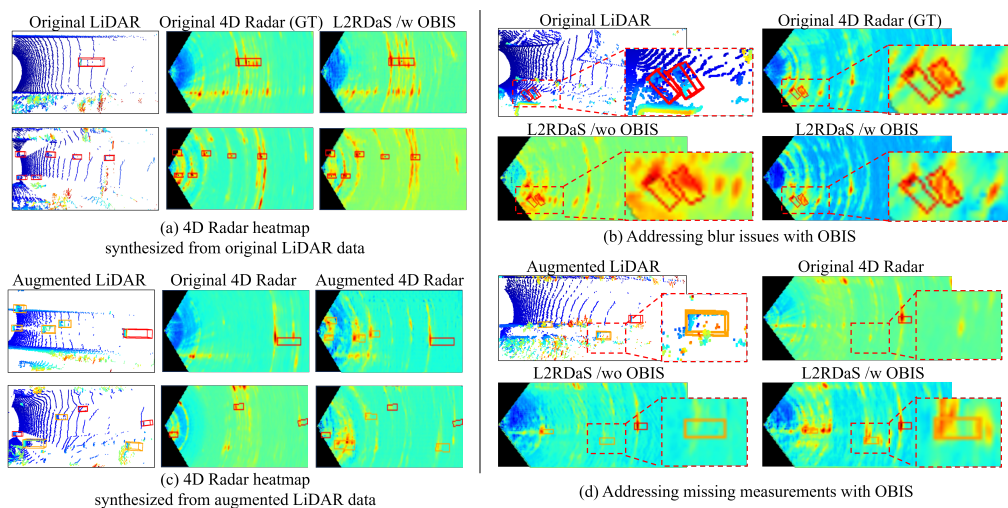


Figure 5: Visualization of L2RDaS with OBIS. Results on non-augmented and augmented LiDAR data, and ablation study on the impact of OBIS.

5.1. Dataset

This study utilizes the K-Radar dataset [2] for training the L2RDaS and applying 4D Radar GT-Aug to train the RTNH [2]. The K-Radar dataset contains 4D Radar data, high-resolution LiDAR and camera data, and ego vehicle data (RTK-GPS, IMU) collected under various weather conditions (clear, cloudy, foggy, rainy, sleet, light snow, heavy snow) and road environments (highways, urban areas, alleyways, campuses, etc.). The dataset uniquely provides 4D Radar tensor data (4DRT) with range, azimuth, elevation, and Doppler dimensions. For L2RDaS training, 3D tensor data (3DRT-XYZ) was used, which was generated by mean pooling the Doppler dimension

of 4DRT and converting it to the Cartesian coordinate system through interpolation. This 3DRT-XYZ data was then transformed into point cloud data using the Percentile method to retain the measurement patterns within the tensor structure, preserving features such as sidelobes, while enhancing training and inference efficiency for RTNH.

5.2. Implementation Details

To validate the proposed GT-Aug, the 4D Radar object detection model RTNH [2] was used, and experiments were conducted using the K-Radar dataset. Performance evaluation was conducted according to the four experimental conditions specified in Table 1 (M1 M4). The K-Radar dataset was modified by expanding the target classes from a single Sedan class to Sedan and Bus/Truck, and by extending the ROI along the y-axis from $[-6.4, 6.4]$ to $[-16, 16]$, while keeping the x-axis and z-axis ranges unchanged at $[0, 72]$ and $[-2, 6]$, respectively. Since L2RDaS synthesizes 4D Radar data from LiDAR data, experiments were conducted under clear weather conditions. During GT-Aug, the object density was set to six (four Sedans and two Bus/Trucks), doubling the original object density of approximately three. The model training utilized an NVIDIA 3090 GPU with a batch size of 8, using the Adam optimizer with a learning rate of 0.001 for 20 epochs.

5.3. Metric

To evaluate the performance of the 4DR GT-Aug, mean average precision (mAP) based on intersection over union (IoU) was employed. The experiments measured mAP for BEV (mAP_{BEV}) and 3D bbox predictions (mAP_{3D}), considering detections with an IoU value of 0.3 or higher as true positives (TP) [35].

5.4. Result

Table 1 demonstrates the effectiveness of the proposed 4DR GT-Aug (M4) in improving RTNH [2] performance. Compared to the baseline M1 (training with original data only), M4 achieved 4.38 percentage points improvement in mAP_{BEV} and 1.54 percentage points in mAP_{3D} . These results indicate that GT-Aug can be effectively applied to 4D Radar tensor data, and the performance improvement suggests that synthesized 4D Radar tensor data maintains radar characteristics necessary for augmentation. Since GT-Aug on the synthesized data improved performance rather than degrading it, this indirectly supports that L2RDaS preserves key distribution properties of real

4D Radar measurements. Compared to M2, which applies conventional GT-Aug, M4 further improved mAP_{BEV} by 1.54 percentage points and mAP_{3D} by 0.61 percentage points, indicating that considering sidelobes and incorporating information beyond GT bboxes, rather than simply copying data within them, is more effective for 4D Radar augmentation. Additionally, M4 outperformed M3, despite both using the same composition of original and synthesized data. The 3.63 percentage point improvement in mAP_{BEV} and 0.74 percentage point improvement in mAP_{3D} indicate that M3 struggles with generalization, whereas M4 benefits from the synthesized data contributing to a more diverse distribution. This variation enriches the training process, allowing the model to learn broader feature representations and ultimately improving detection performance.

Table 1: Comparison of mAP scores across BEV and 3D (Sedan and Bus/Truck). M1: Training with original data only. M2: Applying conventional GT-Aug to match M1 data quantity. M3: Performing the same conventional GT-Aug as M2 but using the same data composition as M4, excluding environments where L2RDaS underperforms (e.g., tunnels, alleys, etc.). M4: Same data as M3 but using the proposed GT-Aug. Results include AP per class and mAP across all classes for BEV and 3D detection. Best results are in bold.

Method	BEV AP \uparrow			3D AP \uparrow		
	mAP	Sedan	Bus/ Truck	mAP	Sedan	Bus/ Truck
M1	38.94	47.19	30.68	34.98	44.60	25.36
M2	41.78	53.42	30.13	35.91	46.14	25.67
M3	39.69	47.00	32.37	35.78	44.82	26.74
M4	43.32	53.16	33.48	36.52	45.85	27.18

5.5. Ablation study

This ablation study validates the rationale behind the L2RDaS design, the necessity of the OBIS, and the importance of the Switcher along with its optimal configuration.

5.5.1. Validation of L2RDaS Module Design

The L2RDaS translates augmented LiDAR data into 4D Radar data, assuming that 3D dense convolution layers in the decoder are effective for generating tensor data. To verify this, experiments compared the use of 3D dense and sparse convolution layers. Input data included original LiDAR

point clouds, with 3D tensor data of 4D Radar as output, compared to original 4D Radar tensor data which is the GT data. Evaluation metrics were peak signal-to-noise ratio (PSNR) and structural similarity index (SSIM), following [12]. Both PSNR and SSIM compare the synthesized data with the GT data, with PSNR measuring the signal-to-noise ratio and SSIM assessing the structural similarity. Both metrics indicate better performance with higher values. Since these metrics are for 2D image data, 3D tensor data was mean-pooled along the height axis for evaluation. Results showed that 3D dense convolution improved PSNR by 0.03dB and significantly enhanced SSIM by 0.09 (approximately 10%), confirming its superiority over sparse convolution for generating tensor data.

Table 2: Validation of decoder layer design in L2RDaS. Using a 3D dense convolution layer in the decoder improves SSIM by over 10% compared to sparse convolution.

Decoder Layer	PSNR (dB) \uparrow				
	All	Highway	Urban	University	Alleyway
3D sparse conv.	20.90	27.24	22.09	24.70	9.57
3D dense conv.	20.93	27.41	22.20	24.53	9.59

(a) PSNR evaluation.

Decoder Layer	SSIM \uparrow				
	All	Highway	Urban	University	Alleyway
3D sparse conv.	0.81	0.87	0.83	0.87	0.68
3D dense conv.	0.90	0.96	0.90	0.94	0.80

(b) SSIM evaluation.

5.5.2. Validation of OBIS Necessity

The OBIS, an additional module for translating augmented LiDAR data into 4D Radar data, is crucial for synthesizing 4D Radar data that closely resembles real-world measurements. To validate its effectiveness, the RTNH model was trained with and without the OBIS, and the object detection performance was compared. The experiments were conducted under conditions optimized for maximum performance, excluding the OBIS. The validation of the OBIS used mAP as the primary evaluation metric. Since there is no direct GT for GT-Aug data, as the data is augmented, the module’s effectiveness was analyzed indirectly through the training results of RTNH. The experimental results showed that adding the OBIS improved object detection performance significantly, with mAP_{BEV} increasing by 3.96% points

and mAP_{3D} by 1.89% points compared to the configuration without OBIS. This demonstrates that OBIS provides essential information to L2RDaS, effectively enhancing the quality of 4D Radar data and the performance of GT-Aug.

Table 3: Validation of object detection performance with OBIS.

Method	BEV AP \uparrow			3D AP \uparrow		
	mAP	Sedan	Bus/ Truck	mAP	Sedan	Bus/ Truck
No OBIS	39.36	51.00	27.71	34.63	43.94	25.31
With OBIS	43.32	53.16	33.48	36.52	45.85	27.18

5.5.3. Validation of Switcher Necessity and Optimal Configuration

The Switcher adjusts the composition of original and augmented data in the training dataset to enhance object detection performance through 4DR GT-Aug. It plays a critical role in balancing these datasets or excluding augmented data in environments where 4D Radar data synthesis is challenging, such as those prone to multi-path effects (e.g., tunnels, narrow alleyways) or other environmental limitations. The term "configuration" refers to the setup of training data composition, specifying the combination of original and augmented data and the application of the Switcher, which directly impacts model performance. Three configurations were tested: (S1) training only with augmented data, (S2) training with equal composition of original and augmented data, and (S3) training with original data in challenging environments and a combination of original and augmented data elsewhere. The results indicated that configurations with the Switcher (S2 and S3) demonstrated superior performance compared to using only augmented data (S1). Notably, S3 (environment-adjusted strategy) achieved the highest performance, with mAP_{BEV} reaching 43.32% and mAP_{3D} reaching 36.52%. These findings highlight the Switcher strategy's effectiveness, as it tailors the training data composition by combining original and augmented data to address environmental challenges such as multi-path effects, ensuring performance.

6. Conclusions

This study proposed the 4D Radar GT-Aug pipeline for augmenting 4D Radar tensor data, integrating L2RDaS, a key module for synthesizing 4D

Table 4: Validation of object detection with Switcher optimization.

Method	BEV AP \uparrow			3D AP \uparrow		
	mAP	Sedan	Bus/ Truck	mAP	Sedan	Bus/ Truck
S1	34.92	44.33	25.51	30.93	41.96	19.90
S2	39.78	52.38	27.17	35.09	45.26	24.91
S3	43.32	53.16	33.48	36.52	45.85	27.18

Radar tensors from LiDAR point clouds, with OBIS and other auxiliary modules. This framework enables augmentation that incorporates both inside and outside GT bboxes, improving object detection performance. Experimental results demonstrated that the proposed pipeline outperformed both non-augmented cases and conventional GT-Aug applied directly to 4D Radar tensor data, with consistent performance gains across all object classes. Additionally, the results confirm that even when applying L2RDaS to synthesize 4D Radar tensor data from LiDAR point clouds, detection performance improves compared to cases without its use. This demonstrates that the proposed model successfully synthesizes radar tensor data from LiDAR, effectively bridging the modality gap and enabling radar-domain GT-Aug. The proposed 4D Radar GT-Aug pipeline lays the groundwork for more effective utilization of 4D Radar in autonomous driving systems, contributing to more robust and reliable object detection technologies. However, L2RDaS exhibits performance limitations in multi-path-prone environments, such as tunnels and alleyways. Future work should address these challenges by developing methods to enhance synthesis robustness across diverse road conditions, incorporate Doppler information, and improve performance under adverse weather scenarios.

References

- [1] D.-H. Paek, J. Guan, Introduction to 4d radar: Hardware, mimo, signal processing, dataset, and ai, in: Tutorial on 2024 IEEE Intelligent Vehicles Symposium, 2024, accessed: 2024-09-18.
URL <https://www.ieee-iv-4dradar.org/>
- [2] D.-H. Paek, S.-H. Kong, K. T. Wijaya, K-radar: 4d radar object detec-

- tion for autonomous driving in various weather conditions, *Advances in Neural Information Processing Systems* 35 (2022) 3819–3829.
- [3] Y. Yan, Y. Mao, B. Li, Second: Sparsely embedded convolutional detection, *Sensors* 18 (10) (2018) 3337.
- [4] X. Huang, P. Wang, X. Cheng, D. Zhou, Q. Geng, R. Yang, The apolloscape open dataset for autonomous driving and its application, *IEEE Transactions on Pattern Analysis and Machine Intelligence* 42 (10) (2020) 2702–2719. doi:10.1109/tpami.2019.2926463.
URL <http://dx.doi.org/10.1109/TPAMI.2019.2926463>
- [5] J. Fang, X. Zuo, D. Zhou, S. Jin, S. Wang, L. Zhang, Lidar-aug: A general rendering-based augmentation framework for 3d object detection, in: *Proceedings of the IEEE/CVF Conference on Computer Vision and Pattern Recognition*, 2021, pp. 4710–4720.
- [6] S. Shi, X. Wang, H. Li, Pointcnn: 3d object proposal generation and detection from point cloud, in: *Proceedings of the IEEE/CVF conference on computer vision and pattern recognition*, 2019, pp. 770–779.
- [7] S. R. System, Smart radar system ir v_16, Tech. rep., Smart Radar System, accessed: 2024-03-02 (August 2023).
URL https://w4.kirs.or.kr/download/broadcast/%EC%8A%A4%EB%A7%88%ED%8A%B8%EB%A0%88%EC%9D%B4%EB%8D%94%EC%8B%9C%EC%8A%A4%ED%85%9C%20IR%20V_16.pdf
- [8] Q. Li, X. Yu, J. Peña Queraltá, T. Westerlund, Multi-modal lidar dataset for benchmarking general-purpose localization and mapping algorithms, arXiv preprint arXiv:2203.03454 (2022).
- [9] Y. Haitman, O. Bialer, BoostRAD: Enhancing object detection by boosting radar reflections, in: *Proceedings of the IEEE/CVF Winter Conference on Applications of Computer Vision*, 2024, pp. 1638–1647.
- [10] P. Isola, J.-Y. Zhu, T. Zhou, A. A. Efros, Image-to-image translation with conditional adversarial networks, in: *Proceedings of the IEEE conference on computer vision and pattern recognition*, 2017, pp. 1125–1134.

- [11] T.-C. Wang, M.-Y. Liu, J.-Y. Zhu, A. Tao, J. Kautz, B. Catanzaro, High-resolution image synthesis and semantic manipulation with conditional gans, in: Proceedings of the IEEE conference on computer vision and pattern recognition, 2018, pp. 8798–8807.
- [12] L. Wang, B. Goldluecke, C. Anklam, L2r gan: Lidar-to-radar translation, in: Proceedings of the Asian Conference on Computer Vision, 2020.
- [13] D.-H. Paek, S.-H. Kong, K. T. Wijaya, Enhanced k-radar: Optimal density reduction to improve detection performance and accessibility of 4d radar tensor-based object detection, in: 2023 IEEE Intelligent Vehicles Symposium (IV), IEEE, 2023, pp. 1–6.
- [14] S.-H. Kong, D.-H. Paek, S. Lee, Rtnh+: Enhanced 4d radar object detection network using two-level preprocessing and vertical encoding, IEEE Transactions on Intelligent Vehicles (2024).
- [15] J. S. Kulpa, Ł. Maślikowski, M. Malanowski, Filter-based design of noise radar waveform with reduced sidelobes, IEEE Transactions on Aerospace and Electronic Systems 53 (2) (2017) 816–825.
- [16] J. Rebut, A. Ouaknine, W. Malik, P. Pérez, Raw high-definition radar for multi-task learning, in: Proceedings of the IEEE/CVF Conference on Computer Vision and Pattern Recognition, 2022, pp. 17021–17030.
- [17] F. J. Harris, On the use of windows for harmonic analysis with the discrete fourier transform, Proceedings of the IEEE 66 (1) (1978) 51–83.
- [18] R. B. Blackman, J. W. Tukey, The measurement of power spectra from the point of view of communications engineering—part i, Bell System Technical Journal 37 (1) (1958) 185–282.
- [19] J. Borkowski, A. Matusiak, Power-of-sine windows as generalized maximum sidelobe decay windows—theory and properties: A review and new results, Online, available at: <https://metrology.wat.edu.pl> (2024).
- [20] R. Weston, O. P. Jones, I. Posner, There and back again: Learning to simulate radar data for real-world applications, in: 2021 IEEE international conference on robotics and automation (ICRA), IEEE, 2021, pp. 12809–12816.

- [21] E. C. Fidelis, F. Reway, H. Ribeiro, P. L. Campos, W. Huber, C. Icking, L. A. Faria, T. Schön, Generation of realistic synthetic raw radar data for automated driving applications using generative adversarial networks, arXiv preprint arXiv:2308.02632 (2023).
- [22] O. Bialer, Y. Haitman, Radsimreal: Bridging the gap between synthetic and real data in radar object detection with simulation, in: Proceedings of the IEEE/CVF Conference on Computer Vision and Pattern Recognition, 2024, pp. 15407–15416.
- [23] P. A. Rangaraj, T. Alkanat, A. Pandharipande, Raids: Radar range-azimuth map estimation from image, depth and semantic descriptions, IEEE Sensors Journal (2025).
- [24] J. Lee, G. Bang, T. Shimizu, M. Iehara, S. Kamijo, Lidar-to-radar translation based on voxel feature extraction module for radar data augmentation, Sensors 24 (2) (2024) 559.
- [25] T. Alkanat, A. Pandharipande, Automotive radar point cloud parametric density estimation using camera images, in: ICASSP 2024-2024 IEEE International Conference on Acoustics, Speech and Signal Processing (ICASSP), IEEE, 2024, pp. 8636–8640.
- [26] W.-J. Jung, D.-H. Paek, S.-H. Kong, 4dr p2t: 4d radar tensor synthesis with point clouds, arXiv preprint arXiv:2502.05550 (2025).
- [27] Y. Zhou, O. Tuzel, Voxelnet: End-to-end learning for point cloud based 3d object detection, in: Proceedings of the IEEE conference on computer vision and pattern recognition, 2018, pp. 4490–4499.
- [28] O. Ronneberger, P. Fischer, T. Brox, U-net: Convolutional networks for biomedical image segmentation, in: Medical image computing and computer-assisted intervention–MICCAI 2015: 18th international conference, Munich, Germany, October 5-9, 2015, proceedings, part III 18, Springer, 2015, pp. 234–241.
- [29] B. Liu, M. Wang, H. Foroosh, M. Tappen, M. Pensky, Sparse convolutional neural networks, in: Proceedings of the IEEE conference on computer vision and pattern recognition, 2015, pp. 806–814.

- [30] B. Graham, M. Engelcke, L. Van Der Maaten, 3d semantic segmentation with submanifold sparse convolutional networks, in: Proceedings of the IEEE conference on computer vision and pattern recognition, 2018, pp. 9224–9232.
- [31] D. Lee, J. Kim, Resolving class imbalance for lidar-based object detector by dynamic weight average and contextual ground truth sampling, in: Proceedings of the IEEE/CVF Winter Conference on Applications of Computer Vision, 2023, pp. 682–691.
- [32] J. Zhan, T. Liu, R. Li, J. Zhang, Z. Zhang, Y. Chen, Real-aug: Realistic scene synthesis for lidar augmentation in 3d object detection, arXiv preprint arXiv:2305.12853 (2023).
- [33] J. Oh, J. Lee, W. Byun, M. Kong, S. H. Lee, False positive sampling-based data augmentation for enhanced 3d object detection accuracy, arXiv preprint arXiv:2403.02639 (2024).
- [34] I. Shumailov, Z. Shumaylov, Y. Zhao, N. Papernot, R. Anderson, Y. Gal, Ai models collapse when trained on recursively generated data, *Nature* 631 (8022) (2024) 755–759.
- [35] A. Geiger, P. Lenz, R. Urtasun, Are we ready for autonomous driving? the kitti vision benchmark suite, in: 2012 IEEE conference on computer vision and pattern recognition, IEEE, 2012, pp. 3354–3361.